The observation of quantum confinement enhancement of the luminescence of nanocystalline $(Y_{0.95}Tb_{0.05})_2O_3$ synthesized by alkalide reduction

Olivera Zivkovic and Michael J. Wagner*

Received 21st January 2008, Accepted 20th March 2008
First published as an Advance Article on the web 8th April 2008
DOI: 10.1039/b801038b

Nanocrystalline $(Y_{0.95}Tb_{0.05})_2O_3$ has been synthesized by sub-ambient homogenous reduction using alkalide solutions, subsequent oxidation and annealing. As synthesized, the material consists of free flowing, agglomerates of ill-defined, amorphous or subnanocrystalline nanoparticles. Samples annealed at 500 °C or greater are crystalline, consisting of agglomerated nanocrystals. The nanocrystals grow from an average of ~1–2 nm to 19 nm and the agglomerates break-up as the annealing temperature is raised from 500 to 1000 °C. The nanocrystalline product displays luminescence typical of the Tb^{3+} ion. The photoluminescence intensity of the green $^5D_4$–$^7F_4$ transition increases with increasing annealing temperature, reaching a maximum of 4% for the nanophosphor annealed at 1000 °C. Evidence of quantum confinement luminescence enhancement is observed for the nanocrystallites annealed at 500 °C, but the quantum efficiency is low, presumably due to their very small size and consequent rapid surface recombination. The results of this study suggest that nanocrystallites of $(Y_{0.95}Tb_{0.05})_2O_3$ with a large quantum confinement fluorescence enhancement may be accessible by appropriate annealing in the temperature range 500–600 °C.

Introduction

Field emission displays (FEDs) are a next generation flat panel monitor technology that will require phosphors that are capable of low voltage excitation if they are to be used in mobile applications.[1] Traditional phosphors typically have high dielectric strength and thus shallow electron penetration depth, necessitating the use of a high potential (typically 10–30 kV) electron beam to achieve sufficient activation; low voltages (≤5 kV) result in the excitation of only a small fraction of the phosphor. The most obvious solution to this problem is to reduce the size of the phosphors so that the physical dimensions of a single grain are of the order of the penetration depth of the electron beam at the operation voltage of the display. However, this requires nanoscale phosphors, making the study of their synthesis and photophysical properties essential to the development of low voltage FEDs. Additional benefits may come with the use of nanoscale phosphors including smoother films with higher fill, increased resolution and luminescence enhancement due to quantum confinement.[2–8]

Oxide phosphors are preferred for FEDs as non-oxides tend to releases gases under electron beam excitation that can poison the field emitting tips.[1,9] Lanthanide doped yttria is an excellent candidate for FED phosphors as they are extremely stable in an electron beam and the efficient narrow emission of the lanthanide ion offers high color purity. Doped with terbium, yttria becomes an efficient green phosphor, Y_2O_3:Tb, a candidate for one third of the color triad necessary for FED operation. The synthesis of nanoscale Y_2O_3:Tb by sol–gel,[5] unspecified microemulsion techniques,[10,11] and combustion[12] has been reported by other investigators. Earlier, we reported the phase transformation of nanocrystalline $(Y_{0.95}Tb_{0.05})_2O_2CO_3$ as an indirect route to nanocrystalline $(Y_{0.95}Tb_{0.05})_2O_3$.[13] Here we present a direct route to $(Y_{0.95}Tb_{0.05})_2O_3$ by post-alkalide reduction oxidation of $Y_{0.95}Tb_{0.05}$ alloy nanoparticles and a comparison of the luminescent properties of the material made by indirect and direct synthetic routes.

The George Washington University, Department of Chemistry, Washington, DC 20052

Experimental

Nanoscale yttrium–terbium metal alloy was synthesized by homogeneous alkalide reduction according to the following scheme:

$$3K^+(\text{15-crown-5})_2Na^- + 1.9YCl_3 + 0.1TbCl_3 \overset{\text{THF}}{\underset{-40^\circ C}{\Rightarrow}} 2(Y_{0.95}Tb_{0.05})_{nano} + 3K^+(\text{15-crown-5})_2Cl^- + 3NaCl$$

Direct exposure of the product to air results in oxidation that generates sufficient heat to decompose the crown ether by-product, making it very difficult to remove by washing. Thus, oxidation of the alloy was performed in two stages. First, a thin layer of the raw product was formed by spreading it onto aluminium foil in an inert atmosphere glove box prior to exposing it to air. Once removed from the glove box, the material was immediately immersed in aerated H_2O at ambient temperature that was used to further oxidize the product and remove the by-products. This two-step oxidation process was highly reproducible in that decomposition of the organic by-products was avoided in all batches allowing complete removal by washing and is more convenient than aerobic addition of water followed by aeration. The product was separated from the wash by centrifuge (15 500 xG). Washing was repeated 10 times to ensure complete removal of the by-products.

YCl_3 and $TbCl_3$ (both anhydrous, 99.99%, packed under argon) were purchased from Aldrich and crown ether (15-crown-5, 98%) was purchased from Alfa-AESAR. Tetrahydrofuran (THF, 99.9+% HPLC grade, inhibitor free) was purified by stirring over KNa alloy until a persistent blue solution was obtained. Reaction vessel loading was performed in a N_2 filled dry box (<1 ppm H_2O and O_2) and solvent transfers were accomplished by vacuum techniques (1×10^{-6} torr). Samples (~0.2 g) were annealed in a tube furnace after flame sealing under vacuum (1×10^{-6} Torr) in fused-silica tubes (interior volume ~46 ml, sample mass to annealing tube volume ratio $\leq 5.7 \times 10^{-3}$ g mL^{-1}). Annealing of larger samples in the given volume resulted in the carbonate rather than the oxide.[13]

Electron micrographs were obtained on a JEM-1200EX transmission electron microscope (TEM) operating at 80 keV. Samples for TEM were dispersed in MeOH by sonication and deposited on Formvar™ holey film/carbon coated copper grids. Powder X-ray patterns were obtained with a Rigaku Miniflex diffractometer (Cu Kα radiation). Infrared spectra were obtained with a Perkin Elmer Spectrum RX FT-IR spectrometer. Elemental analysis was obtained by X-ray fluorescence (Kratos Analytical EDX-700). Photoluminescence measurements were performed on a Shimadzu RF-5301PC Spectrofluorimeter at ambient temperature. Quantum yields were determined by comparison with the photoluminescence of sodium salicylate excited at the same wavelength as the corresponding sample.[14,15]

Results and discussion

The material obtained after washing with aerated H_2O is a free flowing white powder. Elemental analysis found the Tb doping level to be 5%, unchanged from the reaction stoichiometry. Note that 5% is not necessarily the optimal doping fraction for maximum quantum yield for this material and no effort was made to optimize this parameter, however the fraction is similar to fractions found to be highly luminescent in the bulk material. FT-IR spectra show that while the material is free of organic by-products, it does contain a significant quantity of adsorbed CO_2. Powder X-ray diffraction (XRD) showed only broad features indicating that the particles are either amorphous or subnanocrystalline.

Annealing the material for 4 h at temperatures as high as 400 °C resulted in no significant change in the powder XRD; material that was annealed for 4 h at 500 °C displayed a broad crystalline pattern consistent with cubic $(Y_{0.95}Tb_{0.05})_2O_3$ (Fig. 1). Annealing in sealed, evacuated fused-silica tubes was necessary to prevent the oxidation of Tb^{+3} to Tb^{+4}, changing the color of the material from white to orange and resulting in a product that displays no fluorescence. Annealing under active vacuum, rather than sealed tubes, resulted in a dark product that also does not fluoresce, presumably due to loss of oxygen from the Y_2O_3 structure. Note that the annealing of the previously unheated material evolves a significant quantity of CO_2, which, as we previously reported, results in the synthesis of the carbonate $(Y_{0.95}Tb_{0.05})_2O_2CO_3$ if the headspace in the sealed ampoule is insufficient, causing a buildup of many atmospheres of pressure.[13] Avoiding the production of the carbonate and instead producing the oxide requires one to limit the pressure that is developed in the ampule as CO_2 is desorbed from the starting material during heating. By decreasing the sample mass to ampoule volume ratio from 0.033 g ml^{-1} in the previous study, to 0.0057 g ml^{-1} in the current study, and consequently the pressure from the evolution of CO_2 during heating from ~4.2 to ~0.72 atm at 400 °C, the carbonate phase is avoided and the oxide results instead.

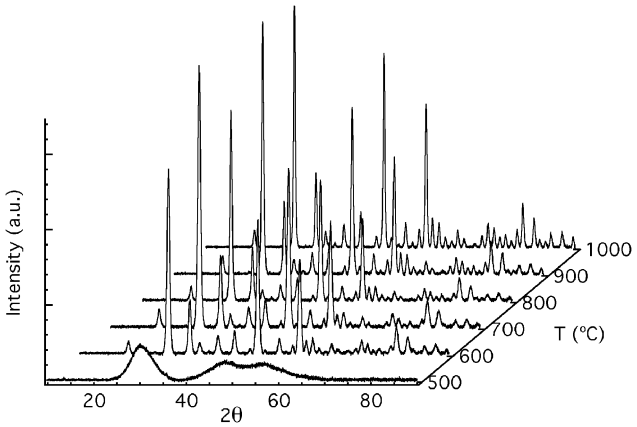

Fig. 1 Powder X-ray diffraction patterns of $(Y_{0.95}Tb_{0.05})_2O_3$ nanocrystallites annealed for 4 h at the indicated temperatures.

Further annealing the material at higher temperatures results in the sharpening of the powder XRD pattern indicating nanocrystallite growth (Fig. 1). Examination of the XRD patterns reveals $(Y_{0.95}Tb_{0.05})_2O_3$ with no other phases detectable (Fig. 2). The crystallite size, as determined from XRD line broadening, is 12.5 nm after annealing at 600 °C and shows no significant change after annealing at 700 °C (Fig. 3). The crystallite size grows linearly with increasing annealing temperature above 700 °C, reaching 19.1 nm after annealing at 1000 °C.

The unannealed material was found to be composed of ill-defined agglomerates in which it is difficult to distinguish individual nanoparticles as was seen in our previous studies of lanthanide doped yttria.[13,16] Annealing the material results in the break-up of these agglomerates to form more defined

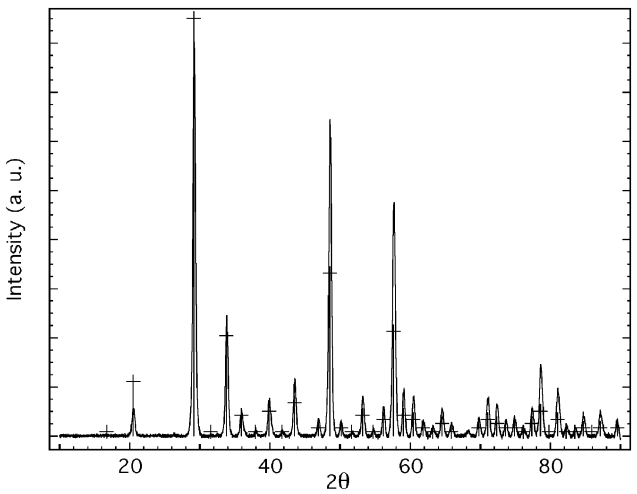

Fig. 2 Powder X-ray diffraction pattern of $(Y_{0.95}Tb_{0.05})_2O_3$ nanocrystals following annealing at 1000 °C for 4 h (solid line) and the standard pattern (JCPDS PDF #25-1011, sticks with crosses).

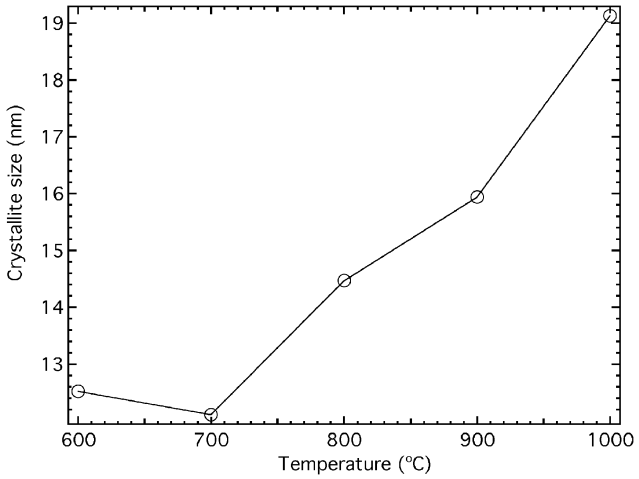

Fig. 3 Average crystalline size determined from X-ray line broadening of the nanocrystalline $(Y_{0.95}Tb_{0.05})_2O_3$ (circles) annealed for 4 h at the given temperature. The lines connecting data points are to guide the eye.

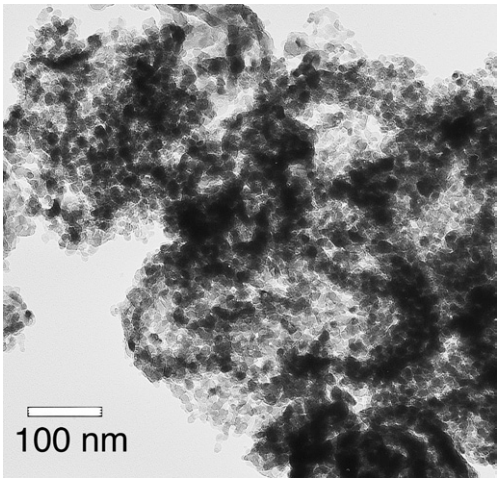

Fig. 5 TEM micrograph of nanocrystalline $(Y_{0.95}Tb_{0.05})_2O_3$ after annealing at 600 °C for 4 h.

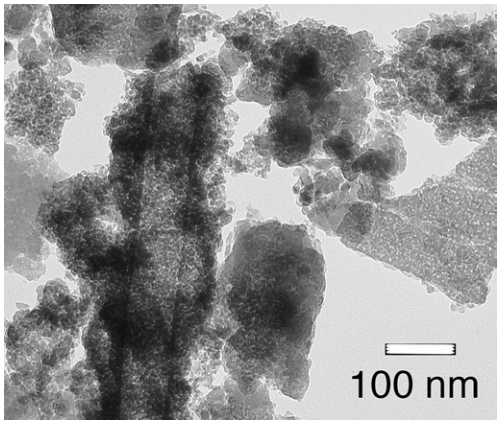

Fig. 4 TEM micrograph of $(Y_{0.95}Tb_{0.05})_2O_3$ nanocrystal agglomerates after annealing at 500 °C for 4 h.

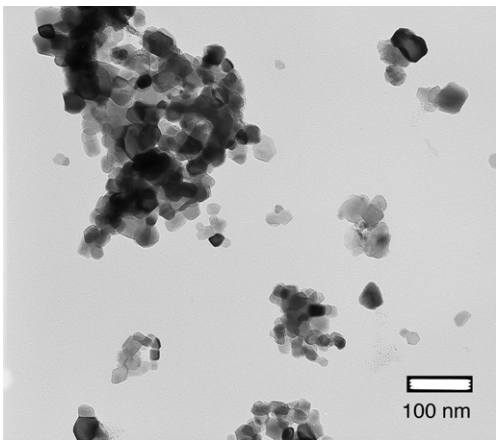

Fig. 6 TEM micrograph of nanocrystalline $(Y_{0.95}Tb_{0.05})_2O_3$ after annealing at 1000 °C for 4 h.

nanoparticles. Typical dimensions of the individual particles are ~4–8 nm following annealing at 500 °C (Fig. 4). Diffraction results show that these are themselves agglomerates rather than individual nanocrystallites; estimating the upper limit of the crystallite size from XRD line broadening yields a value of less than 2 nm. Dark field TEM micrographs confirm that few crystallites are larger than 2 nm, the vast majority being ~1 nm or smaller. Annealing at 600 °C results in growth of the agglomerates into well defined nanoparticles that have dimensions (~10–14 nm) in good agreement with that determined by powder XRD peak broadening (Fig. 5). Again, dark field TEM micrographs are in agreement, showing that the individual nanoparticles are actually individual nanocrystallites. Annealing at progressively higher temperatures results in nanocrystallite size growth observed in TEM micrographs in good agreement with XRD line broadening results. Annealing at 900 °C results in the nanocrystalline agglomerates loosening and beginning to break-up. After annealing at 1000 °C, the majority of the nanocrystallites are ~20 nm in their largest dimension, although some as large as ~30 nm and as small as ~10 nm can be observed in the TEM micrograph (Fig. 6).

Photoluminescence spectra display emission typical of transitions $^5D_4$–^7F_J of the Tb^{3+} ion (Fig. 7). Featureless emission peaks are observed for unannealed material; peak structure consistent with sublevels due to crystal field splitting can be observed after annealing the material to 500 °C and higher, coincident with crystallization observed in powder XRD spectra. The quantum efficiency of the phosphors increases with increasing nanocrystallite size, as might be expected since the increase in size implies a decrease in surface recombination sites, but is contrary to the findings of other investigators.[5] However, this correlation is not perfect, increasing the annealing temperature from 800 to 900 °C increases the size of the nanocrystallites from 14.5 to 16.0 nm but the quantum efficiency does not increase. This anomalous behavior may be attributed to the loosening and break-up of agglomerates of nanocrystallites observed in TEM micrographs. The increase in quantum efficiency expected due to nanocrystallite growth brought about by annealing at 900 °C could be offset by the loss of surface passivation afforded by agglomeration. Quantum efficiency of the green $^5D_4$–$^7F_4$ transition and the combined quantum efficiency of all of the transitions

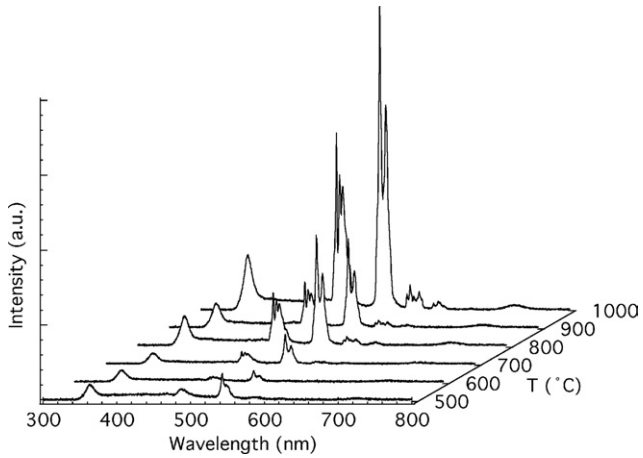

Fig. 7 Photoluminescence spectra of nanocrystalline $(Y_{0.95}Tb_{0.05})_2O_3$ after annealing at the indicated temperatures for 4 h.

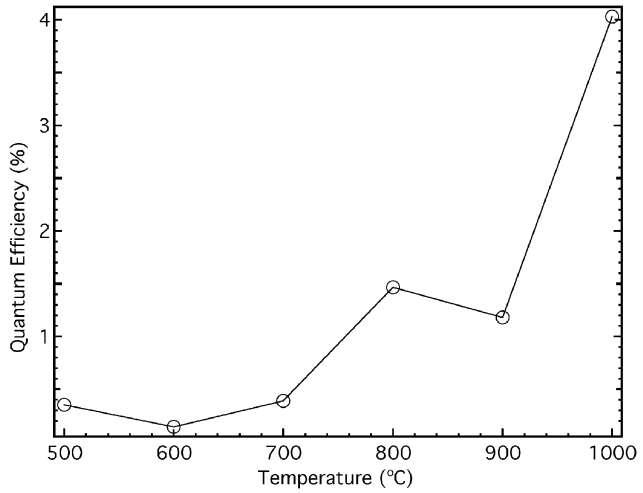

Fig. 8 Quantum efficiency for the $^5D_4$–$^7F_4$ transition of the nanophosphors excited at their wavelength of maximum efficiency (see Fig. 9) plotted as a function of annealing temperatures. The lines connecting data points are to guide the eye.

reaches maxima of 4.0 and 9.7% respectively following annealing at 1000 °C (Fig. 8).

The excitation spectrum of the $(Y_{0.95}Tb_{0.05})_2O_3$ made by direct synthesis exhibits one peak centered at 233 nm prior to annealing, shifting to 248 nm after annealing at 500 °C, coincident with crystallization (Fig. 9). The spectrum of material annealed at 600 °C exhibits two peaks, at 304 and 278 nm respectively, assigned to 4f–5d transitions.[12] The spectra of samples annealed from 600 to 900 °C are essentially identical when scaled to normalize quantum efficiency. The ratio of the 304 and 278 nm peak intensities changes from 0.94 : 1 to 1.12 : 1 after annealing at 1000 °C but the peak shape is invariant. Comparison of the excitation spectra of the $(Y_{0.95}Tb_{0.05})_2O_3$ synthesized by direct and indirect [through a $(Y_{0.95}Tb_{0.05})_2O_2CO_3$ precursor] routes shows that in addition to the 304 and 278 nm peaks, a large peak at 243 nm can be observed in the spectra of the material made by the indirect route. The ratio of the 304 and 278 nm peak intensities is 1.34 : 1 for the material made by indirect synthesis, larger

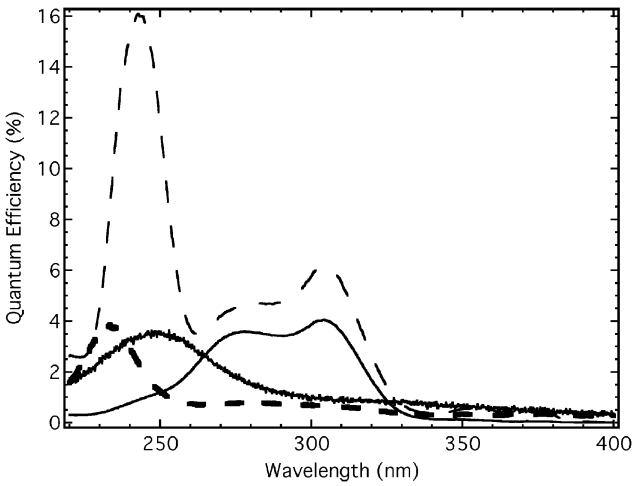

Fig. 9 Photoluminescence quantum efficiency for the $^5D_4$–$^7F_4$ transition of unannealed nanoparticulate material (heavy dashed line) and nanocrystalline $(Y_{0.95}Tb_{0.05})_2O_3$ after annealing at 500 °C (heavy solid line) and 1000 °C (solid line) for 4 h plotted as a function of excitation wavelength. The quantum efficiencies of the unannealed and 500 °C data have been multiplied by a factor of 10 for clarity. Data previously published for nanocrystalline $(Y_{0.95}Tb_{0.05})_2O_2CO_3$ annealed at 1000 °C for 4 h (dashed line) is also shown for comparison.[13]

than seen for that by the direct route. These 4f–5d transition peak positions are similar to that seen for bulk material but the ratio is significantly different; the 278 nm peak intensity is much larger than that of the 304 nm peak for the bulk material.[11]

The 248 nm peak in the excitation spectra of directly synthesized $(Y_{0.95}Tb_{0.05})_2O_3$ annealed at 500 °C is not present when the material is annealed at higher temperature but is similar to that observed at 243 nm in the excitation spectra of $(Y_{0.95}Tb_{0.05})_2O_3$ made by the indirect method and that of $(Y_{0.95}Tb_{0.05})_2O_2CO_3$ at 247 nm.[13] A very similar feature was reported for nanocrystalline Y_2O_3:Tb made by an unspecified microemulsion technique and is absent in the spectra of bulk samples; it has been suggested that the feature arises from quantum confinement occurring in nanocrystals less than 5 nm in diameter.[10] It should be noted that the model of quantum confinement suggested is markedly different to that widely invoked to explain the behavior of semiconductor nanomaterials and the reader is cautioned to read the referenced literature[10] to fully understand the analysis in this report.

The quantum confinement model could explain why the 248 nm peak observed in the excitation spectra of $(Y_{0.95}Tb_{0.05})_2O_3$ annealed at 500 °C disappears upon annealing at 600 °C, the spectra becoming more "bulk-like". The crystallite size grows from <1–2 nm to ~12.5 nm over this annealing temperature range, transforming the material from very small nanocrystallites that are predicted to exhibit quantum confinement to ones that are postulated to be too large. Also supporting this explanation is the decrease in the maximum quantum efficiency of the green $^5D_4$–$^7F_4$ transition from 0.352 to 0.144% observed when increasing the annealing temperature from 500 to 600 °C. The low quantum efficiency for the material exhibiting quantum confinement could well be due to the extremely small nanocrystallite size; with most of the nanocrystallites being less than 1 nm in their largest dimension, increased surface recombination

may negate the quantum enhancement. Another of our observations appears to contradict this model; $(Y_{0.95}Tb_{0.05})_2O_3$ made by the indirect method has an average crystallite size measured by XRD line broadening far in excess of 5 nm (22.6 nm after annealing at 1000 °C) yet displays this "quantum confinement" peak in its excitation spectra. However, the measure of crystallite size is misleading; TEM observations found that the material appears to be highly textured, with typical length scales on the order of a few nanometres and thus the photoluminescence enhancement observed is consistent with the quantum confinement model.[13] Note that this enhancement of the 243 nm peak occurs at the expense of the "bulk-like" peaks; the quantum efficiency of the green $^5D_4$–$^7F_4$ transition under 304 nm excitation decreases from 9.3 to 6.1% when the annealing temperature is increased from 800 to 1000 °C and the surface area and texturing increases. The texturing found in the material made by the indirect method, presumably brought about by the release of gas during the transformation from a carbonate to an oxide, is not observed for $(Y_{0.95}Tb_{0.05})_2O_3$ made by the direct method reported here, consistent with the absence of a peak due to quantum confinement.

Comparing the quantum efficiencies of the $(Y_{0.95}Tb_{0.05})_2O_3$ made by direct and indirect synthesis is not without complication. The maximum quantum efficiency of $(Y_{0.95}Tb_{0.05})_2O_3$ made by the direct method (4%) is significantly less than that made by the indirect method (16%). However, this is due to the prominence of the 243 nm peak in the excitation spectrum of the later, consistent with quantum confinement, that is not present in the former. Comparison of the "bulk-like" 304 nm excitation peaks present in samples made by either method after annealing at 1000 °C reveals that the quantum efficiencies are more closely matched, 4.0% and 6.1% for the direct and indirect methods respectively. This difference can be reasonably assumed to be due to the larger average crystallite size of the material made by the indirect (22.6 nm) relative to that made by the direct route (19.1 nm).

Conclusions

Nanocrystalline $(Y_{0.95}Tb_{0.05})_2O_3$ can be synthesized directly by alkalide reduction followed by oxidative washing and annealing without going through a carbonate intermediate by annealing in sealed tubes with a sample mass to ampoule volume ratio of 0.0057 g ml^{-1} or less. The material is strongly fluorescent after annealing at 1000 °C, however, it displays a maximum quantum yield for the green $^5D_4$–$^7F_4$ transition that is only 25% of that observed for material made by transformation of a carbonate intermediate. This difference can be reasonably assigned to the highly textured morphology of the indirectly synthesized material, having surface feature length scales of a few nanometres, resulting in quantum confinement fluorescence enhancement. Similar enhancement was observed in material made directly and annealed at 500 °C, albeit with a low quantum efficiency. This study suggests that the quantum confinement might be optimized in this material by altering the annealing regime to find an optimal temperature between 500 and 600 °C, obtaining nanocrystallites that are small enough to allow for quantum confinement but large enough to minimize surface recombination.

Acknowledgements

We thank the National Science Foundation for financial support (DMR-0504925).

References

1 P. H. Holloway, T. A. Trottier, B. Abrams, C. Kondoleon, S. L. Jones, J. S. Sebastian, W. J. Thomes and H. Swart, *J. Vac. Sci. Technol., B*, 1999, **17**, 758–764.
2 B. M. Tissue, *Chem. Mater.*, 1998, **10**, 2837–2845.
3 J. D. Holmes, K. J. Ziegler, R. C. Doty, L. E. Pell, K. P. Johnston and B. A. Korgel, *J. Am. Chem. Soc.*, 2001, **123**, 3743–3748.
4 R. N. Bhargava, D. Gallagher, X. Hong and A. Nurmikko, *Phys. Rev. Lett.*, 1994, **72**, 416–419.
5 E. T. Goldburt, B. Kulkarni, R. N. Bhargava, J. Taylor and M. Libera, *J. Lumin.*, 1997, **72–74**, 190–192.
6 G. Wakefield, H. A. Keron, P. J. Dobson and J. L. Hutchison, *J. Colloid Interface Sci.*, 1999, **215**, 179–182.
7 P. K. Sharma, M. H. Jilavi, R. Nass and H. Schmidt, *J. Lumin.*, 1999, **82**, 187–193.
8 V. Jungnickel and F. Henneberger, *J. Lumin.*, 1996, **70**, 238–252.
9 S. Itoh, H. Toki, Y. Sate, K. Morimoto and T. Kishino, *J. Electrochem. Soc.*, 1991, **138**, 1509.
10 R. N. Bhargava, V. Chhabra, B. Kulkarni and J. V. Veliadis, *Phys. Status Solidi B*, 1998, **210**, 621–629.
11 Y. L. Soo, S. W. Huang, Y. H. Kao, V. Chhabra, B. Kulkarni, J. V. Veliadis and R. N. Bhargava, *Appl. Phys. Lett.*, 1999, **75**, 2464–2466.
12 J. Wang, H. Song, B. Sun, X. Ren, B. Chen and W. Xu, *Chem. Phys. Lett.*, 2003, **379**, 507–511.
13 O. Zivkovic, K. E. Mooney and M. J. Wagner, *Chem. Mater.*, 2007, **19**, 3419–3424.
14 J. Tregellas-Williams, *J. Electrochem. Soc.*, 1958, **105**, 173–178.
15 R. Allison, J. Burns and A. J. Tuzzolino, *J. Opt. Soc.*, 1964, **54**, 747–751.
16 J. A. Nelson, E. L. Brant and M. J. Wagner, *Chem. Mater.*, 2003, **15**, 688–693.

